Reprinted from Analytical Chemistry 1989, *61*, 1029.
Copyright © 1989 by the American Chemical Society and reprinted by permission of the copyright owner.

Threshold Conditions of Plasma Ignition in Laser Ionization Mass Spectrometry of Solids

Akos Vertes*,[1] and Marc De Wolf

Department of Chemistry, University of Antwerp (U.I.A.), Universiteitsplein 1, B-2610 Wilrijk, Belgium

Peter Juhasz

Central Research Institute for Physics of the Hungarian Academy of Sciences, P.O. Box 49, H-1525 Budapest 114, Hungary

Renaat Gijbels

Department of Chemistry, University of Antwerp (U.I.A.), Universiteitsplein 1, B-2610 Wilrijk, Belgium

The adiabatic absorption model has been introduced in order to draw a line between the two well-known regimes of laser ionization: laser desorption and laser plasma ionization. Our threshold definition made it possible to calculate threshold laser irradiances for CO_2, ruby, and quadrupled Nd-YAG lasers and for different materials characterized by wide ranges of number density, molar absorption coefficient of the target, and ionization potential. The effect of these parameters was studied and the absorption coefficient was found to be the most important one. Decreasing the absorption coefficient elevates the energy per unit area required to reach plasma ignition but, surprisingly, lowers the threshold temperature. Comparison with scattered experimental findings indicates that some other mechanisms may give rise to lower laser intensity requirements for plasma formation. Among them two possible mechanisms were investigated: the Poole–Frenkel effect due to the high external electric field generated by the light pulse itself, and the Debye correction related to screening effects in the plasma. Both mechanisms can explain up to ~50% depression in the threshold energy. The Poole–Frenkel effect is more important in the case of weakly absorbing materials, whereas the Debye correction dominates in the case of strongly absorbing targets.

*To whom correspondence should be addressed.
[1] On leave from: Central Research Institute for Physics of the Hungarian Academy of Sciences, Budapest, Hungary.

INTRODUCTION

Laser ionization has established a considerable role in the mass spectrometry of solids during the last decade. For its flexibility in switching between different ionization modes it is used in commercial instruments, not only as a mild ionization technique producing mainly quasi-molecular ions of nonvolatile organic compounds but also as a complete atomization source for determination of the elemental composition of inorganic samples. Laser ionization sources are combined with different mass spectrometer systems ranging from time of flight setups through double focusing instruments to Fourier transform ion cyclotron resonance analyzers.

It is well-known from experimental (*1*, *2*) and theoretical studies (*3*) that two limiting cases of laser ionization exist; they can be distinguished by the amount of energy which is deposited per unit area on the target by a single laser pulse. The processes generated by a low power density laser pulse are usually classified as laser desorption while the high power density limit is referred to as laser plasma ionization. (Light power density is measured in units of W/cm^2 and used as a synonym of light intensity or, more precisely, irradiance throughout the paper.)

The transition between the two limiting modes is usually continuous giving rise to more and more complete fragmentation and/or atomization when the deposited energy increases. On the other hand it is also apparent from the literature—see for instance the matrix assisted ionization experiments (*4*, *5*) or the laser defocusing studies (*6*)—that

0003-2700/89/0361-1029$01.50/0 © 1989 American Chemical Society

some kind of threshold irradiance, separating the limiting regimes, exists.

The definition of this threshold is quite loose and ambiguous both experimentally and theoretically. In ref 4 the concept of threshold irradiance has been introduced in the following way: "... at this value a decrease in irradiance by ~20% only causes the intensities of sample-specific ions to reproducibly and sharply decline by a factor of 10–50 to noise level." It is clear that this definition corresponds to an ultimate lower limit of ion observability in a given setup. Consequently it marks the lower bound of laser desorption of ions rather than the transition between desorption and plasma ionization. The accuracy of the measured values goes with the accuracy of the irradiance measurement and with the noise and sensitivity characteristics of the ion detection system. In ref 4 for instance, irradiance calibration uncertainty was ±50%.

The defocusing experiments show that labile compounds exhibit different spectra depending on focal spot size even if the same power density has been delivered to the target (*6*). (In the experiments the laser shot energy was compensated for spot size changes with twisted polarizers in order to yield the same power density on the target.) A very likely explanation of the spectral changes observed can be the existence of a threshold in light intensity separating different mechanisms of ionization like laser desorption and plasma ionization.

Another obvious distinction between the two regimes is based on the completely different ion kinetic energy distribution patterns observed (*7*). Laser desorption provides ions with quasi-Maxwellian energy distributions characterized typically by a mean kinetic energy of a few electronvolts (*2*), while in the case of laser plasma ionization strongly non-Maxwellian distributions extending well above 100 eV are identified (*8*, *9*).

In this paper we make an attempt to set up a rough model which provides some insight in laser ionization processes and use a number of simplifications in order to establish a distinction between the two above-mentioned regimes. Consequently it becomes possible to estimate the threshold power density and related plasma properties for a large variety of lasers and targets.

THEORY

Adiabatic Absorption Model. In order to trace the fate of energy deposited in the target by a laser pulse, we use the energy conservation formalism of hydrodynamics. In many cases a one-component one-dimensional model can be adopted (*3*) to describe the expansion of the laser-generated plume perpendicular to the target surface

$$\frac{\partial[\rho(e + v^2/2)]}{\partial t} = -\frac{\partial[\rho v(e + p/\rho + v^2/2) - \Phi]}{\partial x} \quad (1)$$

where $v(x,t)$, $p(x,t)$, $\rho(x,t)$, and $\rho(x,t)e(x,t)$ are the velocity, the pressure, the density, and the energy density of the material at coordinate, x, perpendicular to the surface, while $\Phi(x,t)$ denotes the power density of the laser beam. The position and time dependence of the variables are not shown in the equations in order to avoid too long expressions. Heat conductivity can be also included in eq 1, although numerical modeling (*10*) indicates that its influence on plasma heating usually does not exceed a few percent.

For the sake of simplicity we would like to evaluate this expression only for the adiabatic limiting case, i.e. when the light absorption and the resulting simultaneous heating take place much faster than the expansion of the evaporated and ionized material. The two phases of laser–target interaction in the adiabatic absorption approximation are schematically shown in Figure 1. In the first phase light absorption and heating lead to evaporation and ionization of a microvolume

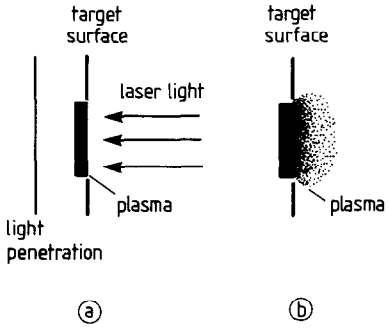

Figure 1. Schematic view of laser–target interaction in the framework of the adiabatic absorption model: (a) adiabatic absorption phase without expansion, (b) expansion phase.

of the target. It is the energy balance of this step which will be the basis of our description. When the laser pulse is over, the second phase starts: free expansion of hot target material. This second part could only be described by means of hydrodynamics (*3*).

In reality the heating and expansion take place simultaneously leading to complicated interaction of the expanding cloud with the laser light. However, our assumption—i.e. decoupling of these processes—does not primarily influence the amount and partitioning of deposited energy between heating and ionization but opens a new channel for energy redistribution. In other words this is equivalent with the simplification that the energy deposited by the laser pulse is converted first to internal energy of the target and subsequently decays partially to kinetic energy.

Accepting this idea we may set $v \equiv 0$ and rewrite eq 1 in the form

$$\frac{\partial(\rho e)}{\partial t} = \frac{\partial \Phi}{\partial x} \quad (2)$$

Using the linearized form of the absorption law, we can express

$$\frac{\partial \Phi}{\partial x} = \alpha\Phi \quad (3)$$

where α, the absorption coefficient of the system, is composed of the absorption of neutrals, α_0, and the absorption of the plasma, α_{pl}

$$\alpha = \alpha_0 + \alpha_{pl} \quad (4)$$

The absorption coefficient of the plasma can be expressed as a function of the number density of free electrons, n_e and electron temperature, T_e (*11*)

$$\alpha_{pl}(n_e,T_e) = \frac{2\omega_l}{c}\,\mathrm{Im}\left(1 - \frac{\omega_{pl}^2}{\omega_l^2\left(1 + \frac{i}{\tau_{ei}\omega_l}\right)}\right)^{1/2} \quad (5)$$

where c is the light velocity, ω_l is the laser frequency, and

$$\omega_{pl} = (4\pi e_0^2 n_e/m_e)^{1/2} \quad (6)$$

is the plasma frequency. τ_{ei} denotes the electron–ion collision time and is expressed as

$$\tau_{ei}^{-1} = \frac{4(2\pi)^{1/2} e_0^4 n_e \ln \Lambda}{3m_e^{1/2}(kT_e)^{3/2}} \quad (7)$$

for singly charged ions. Here e_0 denotes the elementary charge and $\ln \Lambda$ is the so-called Coulomb logarithm, which is determined by

$$\Lambda = \frac{3}{2e_0^3}\left(\frac{k^3 T_e^3}{\pi n_e}\right)^{1/2} \quad (8)$$

according to Spitzer (*12*). The value of ln Λ accounts for the effect of Coulomb interaction in the electron ion scattering process.

For the sake of simplicity we attribute the normal absorption coefficient to electronic and/or vibrational transitions in the neutrals and ions; thus it can be expressed in terms of molar absorption coefficients and number densities

$$\alpha_0 = \alpha' n_{tot}(1 - \eta) + \alpha'' n_{tot}\eta \qquad (9)$$

where η is the degree of ionization and $\alpha' = 1000\epsilon_n/N_A$ is related to the molar absorption coefficient of the neutrals, ϵ_n; a similar relation holds for α'' (ions). To keep the number of free parameters low, we confined the evaluation of our model to the case when the ions have no significant contribution to the light absorption. Similar calculations are easy to carry out in the more general case when both the neutral and the ionic species are absorbing.

The complicated process of light absorption and energy redistribution which is of course position and time dependent can be divided into two spatial regions and two time domains. First the laser heats the target material, producing immediately a plume of target particles. The density and absorptivity of this plume are bounded to their values in the solid, and since the strongest absorption is observed in the interface layer, we may use the bulk values as an approximation for the plume too. As the laser heating goes on, the degree of ionization in the plume increases and sooner or later we will observe the contribution to absorption from plasma particles in the plume.

The internal energy density of an ionized ideal gas has the following form:

$$\rho e = n_{tot}[(3/2)(1 + \eta)kT + \eta U_i] \qquad (10)$$

where $n_{tot} = n_i + n_n$ is the number density of particles in the solid, which approximates the total number density in the plume, composed of the number density of ions and neutrals. $\eta = n_i/n_{tot}$ and U_i denote the energy of ionization. Replacing the internal energy density of the target with that of an ionized ideal gas implies that the heat of melting and vaporization are negligible compared to the ionization energy, an approximation which can be justified for a large number of organic compounds.

Making use of eq 2–4 and 10 and converting the differential equation into its finite difference form, we arrive at

$$n_{tot}[(3/2)(1 + \eta_2)kT_2 + \eta_2 U_i] \approx (\alpha_0 + \alpha_{pl})\Phi\tau_{pulse} \qquad (11)$$

Furthermore, we included the experience that during a laser pulse—powerful enough to ignite a plasma and lasting for τ_{pulse}—the final target temperature, T_2, and the final degree of ionization, η_2, exceed considerably their initial values T_1 and η_1.

At the initial phase of the laser solid interaction, the absorption of the neutrals exceeds the plasma absorption ($\alpha_0 \gg \alpha_{pl}$) since there are very few ions, but as heating and ionization proceed (yielding a partially ionized gas), the absorptivity of the neutrals decreases and α_{pl} increases in this ionized gas. Therefore, our definition of the plasma ignition threshold is the fulfillment of the

$$\alpha_0(\eta) = \alpha_{pl}(n_e, T_e) \qquad (12)$$

condition during the laser shot. The meaning of this criterion is that if a laser pulse can heat and ionize the material up to the point where the importance of plasma absorption surpasses the importance of ordinary absorption, plasma phenomena will dominate the processes. So for different targets and lasers, we are looking for the threshold power density, Φ_{thr}, for which eq 12 holds.

There is another feature we have to consider in order to describe the plasma ignition, namely the relationship between the temperature and the degree of ionization. It is common to use the local thermal equilibrium hypothesis for this purpose. This approximation was supported, at least in the dense regions of the plasma, by detailed hydrodynamic and relaxation time calculations (see ref 3). Consequently, we applied the well-known simplified Saha equation

$$\frac{\eta^2}{1 - \eta} = \frac{1}{n_{tot}}\left(\frac{2\pi k T_e m_e}{h^2}\right)^{3/2} \exp\left(-\frac{U_i}{kT_e}\right) \qquad (13)$$

Combining eq 5–9 and 13 we can evaluate the threshold criterion for plasma ignition, eq 12, and determine threshold values for the temperature, T_{thr}, and for the threshold degree of ionization, η_{thr}. With these values substituted into eq 11 it is possible to determine the threshold power density of a laser shot

$$\Phi_{thr} = \frac{(3/2)(1 + \eta_{thr})kT_{thr} + \eta_{thr}U_i}{2\alpha'(1 - \eta_{thr})\tau_{pulse}} \qquad (14)$$

The energy of ionization can be substituted by the ionization potential; however, in dense plasmas or at elevated light intensities corrections are necessary. For the first approximation of ionization energy in the basic form of the model we used the ionization potential, I_p, values

$$U_i = I_p \qquad (15)$$

This choice, however, does not reflect the special circumstances of ionization in a plasma by light radiation of high intensity. Two effects can be accounted for as corrections to the normal ionization potential, both depressing its value.

Ionization in a plasma takes less energy than for a free particle because of effects similar to ion–ion interaction in electrolytes. This is expressed by the so-called Debye correction (*13*)

$$\Delta E_D = e_0^2/\lambda_D \qquad (16)$$

here

$$\lambda_D = \left(\frac{kT_e}{8\pi n_e e_0^2}\right)^{1/2} \qquad (17)$$

is the Debye length for a plasma having one singly charged ionic component.

The other important correction is due to the high electric field present at elevated light intensities. The Poole–Frenkel effect describes the lowering of ionization energy due to the deformation of the Coulomb potential acting between an electron and the corresponding ion (*14*)

$$\Delta E_{PF} = e_0\left(\frac{4e_0E_0}{\epsilon}\right)^{1/2} \qquad (18)$$

where E_0 is the field strength of the external electric field and ϵ is the dielectric permittivity of the material.

Thus the ionization energy with these corrections can be expressed as

$$U_i = I_p - \Delta E_D - \Delta E_{PF} \qquad (19)$$

We will investigate the effects of the corrections on the ionization and plasma ignition processes, too.

It is worthwhile to notice that the present model is valid only if the main results of energy deposition are target heating and ionization. If a substantial amount of energy is used for melting, evaporation, or fragmentation or if the hydrodynamic effects are not negligible, they have to be included in the energy density formula, eq 10, and the evaluation of the model is not straightforward anymore.

Another class of important restrictions is the exclusion of nonlinear light absorption, as well as nonequilibrium phe-

nomena. Nonlinear absorption can be handled by the extension of the right-hand side of eq 3 with terms proportional to higher powers of the light intensity. Here we confine our discussion to the more common linear absorption.

Nonequilibrium processes are rather difficult to describe. In the case of their presence the temperature of the different species (electrons, ions and neutrals) would be different and local thermal equilibrium (described by eq 13) would not prevail. The correct procedure would be to introduce the kinetic equations for ionization and neutralization. We have found it, however, more appropriate not to include this effect, especially, since we are looking for moderate light intensities where heating rates are just enough to produce threshold ionization and threshold temperature.

RESULTS AND DISCUSSION

The method for the calculation of threshold power density leading to plasma ignition will be outlined in short. The threshold condition, eq 12, together with the Saha equation, eq 13, provides a set of two transcendent equations for the threshold values of the ionization degree and temperature. The solution has to be sought by way of the interval halving iterative method.

According to our earlier remark we set α'' equal to zero in eq 9. Since the threshold value of the ionization degree was usually below 0.1, this simplification did not lead to severe errors. Using the results of the above-mentioned iterative procedure, we could determine the threshold power density by eq 14.

We applied the calculation scheme for three laser wavelengths, namely the quadrupled frequency of the Nd-YAG laser (265 nm), the ruby laser (694 nm), and the CO_2 laser (10.6 μm). Pulse duration for the three lasers was 10, 30, and 150 ns, respectively.

In order to cover as broad a variety of target materials as possible, we surveyed the absorption coefficients (*15*), total number densities (*16*), and ionization potentials (*17*, *18*) of different substances. The absorption coefficient changes roughly between 10^4 (opaque) and 0.1 cm^{-1} (transparent) at a given wavelength. Most ionization potentials vary between 4 and 16 eV while number densities fall in the region of 10^{21}–10^{23} particles/cm^3.

Different classes of materials (insulators, semiconductors, and metals) can be characterized by specific choices of these parameters. Metals usually have low ionization potential (4 eV $\leq I_p \leq$ 9 eV), high absorption coefficient (10^4 $cm^{-1} \leq \alpha_0$), and high number density (10^{22} particles/$cm^3 \leq n_{tot} \leq 10^{23}$ particles/cm^3). The ionization potential of insulators is typically in the range 7 eV $\leq I_p \leq$ 16 eV, while their absorption coefficient depends on whether they are transparent or opaque. Transparent insulators have $\alpha_0 \leq 1$ cm^{-1} and opaque materials have higher values. The number density of insulating materials depends on their structure: densely packed crystals of elements are generally on the more dense side while organic compounds and complex structures exhibit lower number density values ($n_{tot} \leq 2 \times 10^{22}$ particles/cm^3). Semiconductors, in general, have values of the above-mentioned parameters falling between those of metals and insulators.

It should be realized that in the following sections not the threshold power density (measured in W/cm^2) is given but, instead, the threshold energy per unit area (measured in J/cm^2). The latter is obtained by multiplication of the power density with the pulse length of the laser.

We subdivided this section in three parts. First, the basic calculation scheme is used in the way already explained. Extensions are given in the following two parts where correction procedures on the basic scheme are applied.

The Basic Model. The results of the calculation are presented in Figures 2 and 3 for different parameter sets. For the calculations shown in Figure 2 we kept the total density constant at a level of 5×10^{22} particles/cm^3 and focused on the variation of the threshold as a function of the molar

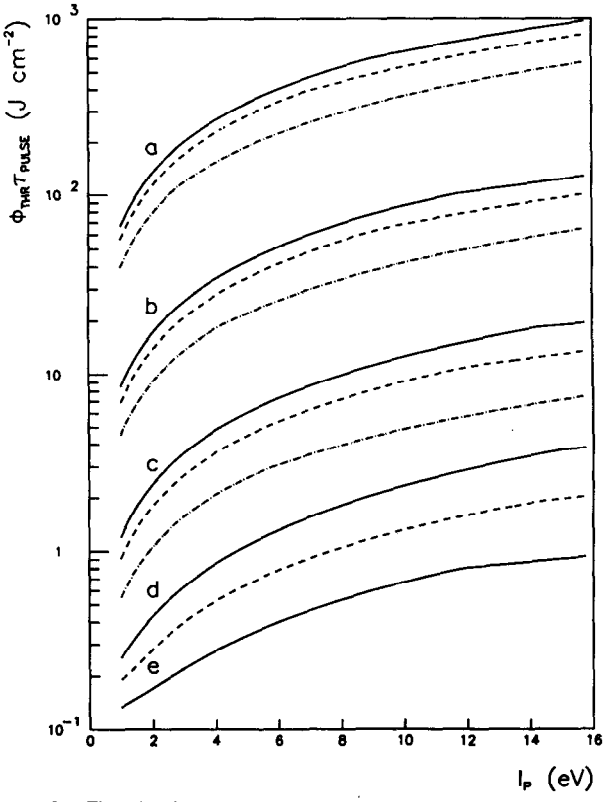

Figure 2. Threshold energy per square centimeter is given as a function of ionization potential using the basic adiabatic absorption model. Three laser types are used: the quadrupled frequency Nd-YAG laser (τ_{pulse} = 10 ns, solid line), the ruby laser (τ_{pulse} = 30 ns, dashed line), and the CO_2 laser (τ_{pulse} = 150 ns, dashed dotted line). See text for explanation.

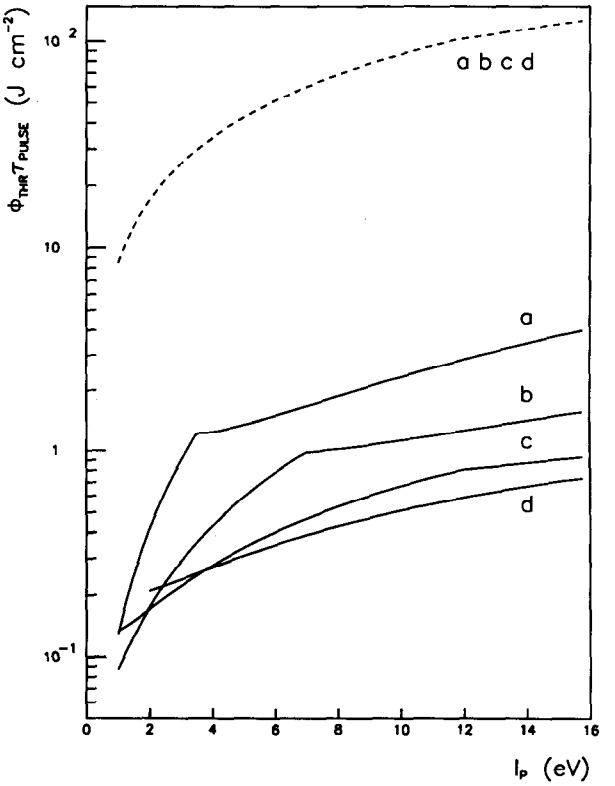

Figure 3. Ionization potential dependence of the threshold energy per square centimeter for materials with different number density of the particles. See text for explanation.

Table I. Measured and Calculated Threshold Energies per Unit Area[a]

	formula	n_{tot}, cm^{-3}	I_p, eV	$\epsilon^{\lambda=266nm}$, L mol^{-1} cm^{-1}	$\Phi_{thr}^{exp}\tau_{pulse}$, J cm^{-2}	$\Phi_{thr}^{theor}\tau_{pulse}$,[c] J cm^{-2}
tryptophan	$C_{11}H_{12}N_2O_2$	3.74×10^{21}	≤7.5	4.5×10^3	0.2	0.91
nicotinic acid	$C_6H_5NO_2$	7.21×10^{21}	9.38	3.4×10^3	0.6	0.79
3-nitrobenzyl alcohol	$C_7H_7NO_3$	5.10×10^{21}	9[b]	8.3×10^3	0.6	1.16

[a] Number densities and ionization potentials are from ref 16 and 18, respectively. The molar extinction coefficients and experimental threshold energy values are given in ref 5. [b] The ionization potential was not available for 3-nitrobenzyl alcohol; therefore we estimated its value on the basis of data for similar molecules. [c] Values are corrected for Poole–Frenkel and Debye effects.

absorption coefficient of the neutrals. We used absorption coefficients 0.1, 1, 10, 100, and 1000 L mol^{-1} cm^{-1} for the curves denoted by a, b, c, d, and e, respectively. An increase of the molar absorption coefficient lowers the threshold (frequently we use the word threshold, instead of threshold energy per unit area, simply for brevity), in general.

It can be noticed from Figure 2 that a decrease of the laser frequency induces a drop in the threshold. By analysis of eq 5 it can be shown that the plasma absorption coefficient will rise if the laser frequency drops. Furthermore, we can conclude that this rise will continue even if the laser frequency falls below the plasma frequency. This tendency is reversed at a certain laser frequency (its value is determined by the collision frequency of the particles in the plasma), and the plasma absorption coefficient will then decay to zero.

Figure 2 also shows an increase of the threshold for materials with increasing ionization potential. Obviously a larger energy fraction of the incoming laser light is necessary for ionizing material with larger ionization potentials, increasing thereby the total amount of deposited energy needed in order to produce the plasma possessing threshold conditions.

In Figure 3, on the other hand, we searched for the influence of the total number density of particles on the threshold. This was performed for two molar absorption coefficient values: one representative of samples with high absorption coefficients (10^3 L mol^{-1} cm^{-1}, solid line) and one for samples with low absorption coefficients (1 L mol^{-1} cm^{-1}, dashed line). Only one laser type, the quadrupled frequency Nd-YAG laser has been investigated. The number density value increased from a toward d, with consecutively 5×10^{21}, 10^{22}, 5×10^{22}, and 10^{23} particles/cm^3. The tendency is noticed that the threshold decreases with increasing particle density, at least for substances with a not too high absorption coefficient.

As we have shown before the threshold will lower with increasing molar absorption coefficient. However, this behavior is not general, as is obvious from Figure 4. Here the calculation is performed with the basic method for the quadrupled frequency Nd-YAG laser. A fixed ionization potential of 9 eV was chosen and the density of the target was set equal to 10^{21} (solid line), 10^{22} (dashed line), and 10^{23} particles/cm^3 (dashed dotted line). A minimum curve is noticed, with the point of reversal being dependent on the material's total density. If we have 10^{21} particles/cm^3 the minimum in the curve is reached at 10^3 L mol^{-1} cm^{-1} and it shifts toward higher absorption coefficients if the material becomes more densely packed.

This peculiar behavior is present in the experimental values in Table I, too. The threshold values are taken from the measurements of Karas et al. (5). These authors verified experimentally that despite the higher molar absorption coefficient of nitrobenzyl alcohol, its threshold irradiance exceeds that of tryptophan. Since the molar absorption coefficients of both products are larger than the one creating minimal threshold, this effect can explain the unexpected findings of Karas et al.

One can also note in Table I the systematic difference between experimental and theoretical values (up to half an order of magnitude) with the theoretical values being higher. The latter were obtained after introducing further corrections to the ionization energy as we will see in the following sections.

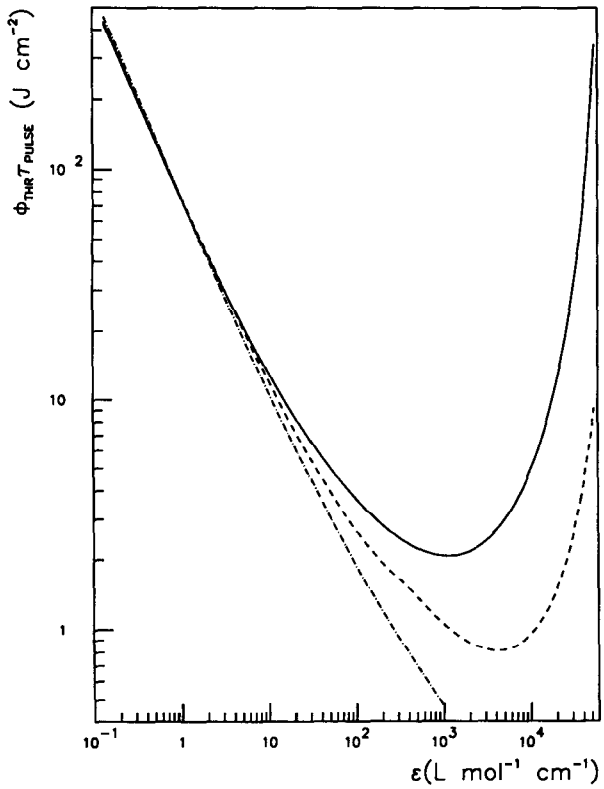

Figure 4. The threshold energy per square centimeter is shown as a function of the absorption coefficient using the basic adiabatic absorption model for quadrupled Nd-YAG laser irradiation.

Both Figures 3 and 4 illustrate that in the case of high molar absorption coefficients—i.e. opaque targets—threshold values are low and variable, whereas poorly absorbing targets show remarkably uniform, but elevated, threshold values. This result prompts the idea that low power density laser ionization can be induced even in the case of transparent samples if they are mixed with better absorbers. The technique is well-known in practice as "matrix assisted laser ionization" and has been applied in the case of nonvolatile organic samples (5).

Before leaving the basic model we emphasize an interesting consequence of our threshold definition. Since the threshold is closely bound to the partition of the deposited energy absorbed by the neutrals and by the plasma, the onset of the plasma regime is strongly related to the magnitude of the normal absorption coefficient. In poorly absorbing materials the absorption of a weakly ionized plasma can already dominate over the normal mechanism, while in the case of good absorbers a strongly ionized plasma is necessary. Therefore, transparent targets exhibit lower threshold temperatures than their opaque counterparts.

Threshold temperatures are displayed in Figure 5 for the same set of targets and lasers as in Figure 2. This finding is

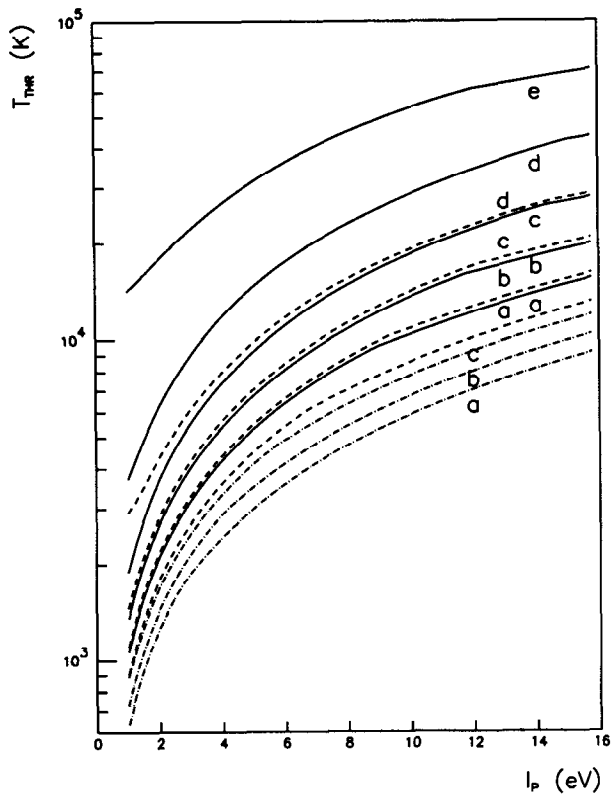

Figure 5. Threshold temperatures for plasma ignition in different targets with various lasers. Laser and material parameters are the same as in Figure 2.

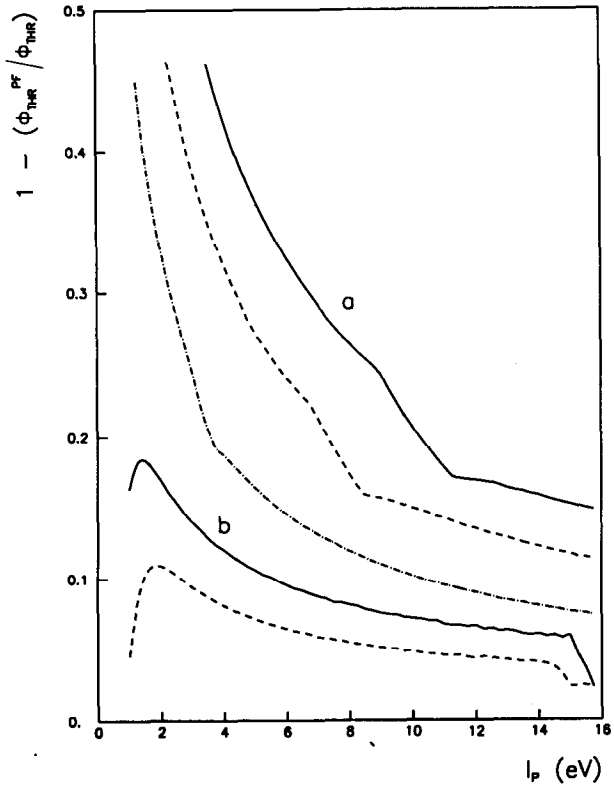

Figure 6. Relative change of the threshold energy per square centimeter is given as a function of the ionization potential using the basic adiabatic absorption model combined with the Poole–Frenkel correction.

straightforward if we recall that a relatively high molar absorption coefficient makes the threshold value of ionization degree increase, also inducing higher threshold temperature because of the local thermal equilibrium condition (eq 13).

Clear demonstration of the above-mentioned phenomenon is apparent from Figure 5: a lower molar absorption coefficient corresponds to a higher threshold energy per unit area in Figure 2 and to a lower threshold temperature as shown in Figure 5.

It is also important to notice that under similar circumstances the threshold temperatures for the frequency quadrupled Nd-YAG laser are always the largest while for the CO_2 laser they exhibit the lowest value. This is in accordance with the widely known observation that UV lasers produce sharply etched craters in the target while increasing laser wavelength creates a molten crater rim.

Apart from the difference in threshold definition (see Introduction) and simplifications in the model which we have already mentioned, there are still some other phenomena—related to the electric field in the laser beam and to the generated plasma—governing the threshold values through the ionization potential. In the next two parts they will be of our concern and their influence will be closely examined.

The Poole–Frenkel Effect. If the laser light penetrates the plasma, it builds up an electric field with a strength given by

$$E_0 = (2\Phi/(\epsilon_0 c))^{1/2} \tag{20}$$

where ϵ_0 denotes the dielectric permittivity of the vacuum. For example, light intensities 10^{10} and 10^6 W/cm^2 generate field strengths 3×10^6 and 3×10^4 V/cm, respectively. From the superposition of the electric field of the radiation and that of the nucleus–free electron interaction, we get a depressed ionization energy given by eq 18. From the formulas it is seen that lowering the power density by 4 orders of magnitude we get a decrease of 1 order of magnitude in the correction of the ionization potential. Thus, this correction for the ionization potential remains reasonably important even at low laser power irradiances.

Figure 6 presents the relation between the corrected threshold energy per unit area and the ionization potential. The correction itself is expressed relative to the threshold. In the model calculations three laser types, the frequency quadrupled Nd-YAG laser (solid line), the ruby laser (dashed line), and the CO_2 laser (dashed dotted line), irradiate a sample which has number density equal to 5×10^{22} particles/cm^3 and molar absorption coefficient of either 0.1 L mol^{-1} cm^{-1} (a curves) or 100 L mol^{-1} cm^{-1} (b curves). In the case of opaque targets irradiated with CO_2 laser, no convergence in the iteration was achieved, but we expect similar behavior to the transparent case, i.e. producing the lowest correction among the three laser types. In general we see declining curves if we pass toward the region of higher ionization potentials, which is equivalent to smaller relative correction values on the threshold.

We can see from Figure 6 that Poole–Frenkel corrections may influence significantly the values of the threshold energy per unit area especially at lower ionization potentials. Here the correction can amount to 45% of the original threshold value. It is also worth mentioning that higher correction can be expected for transparent materials. For opaque targets the Poole–Frenkel corrections do not exceed 15% of the uncorrected threshold and this is usually below the accuracy of the irradiance determination in the experiments.

The Debye Effect. The electric potential, $V(r)$, of a singly charged ion in a plasma is of the form (*13*)

$$V = \frac{e_0}{r} \exp\left(-\frac{r}{\lambda_D}\right) \tag{21}$$

where λ_D is the Debye length, given by eq 17. Since the potential energy of free electrons in the plasma is below their

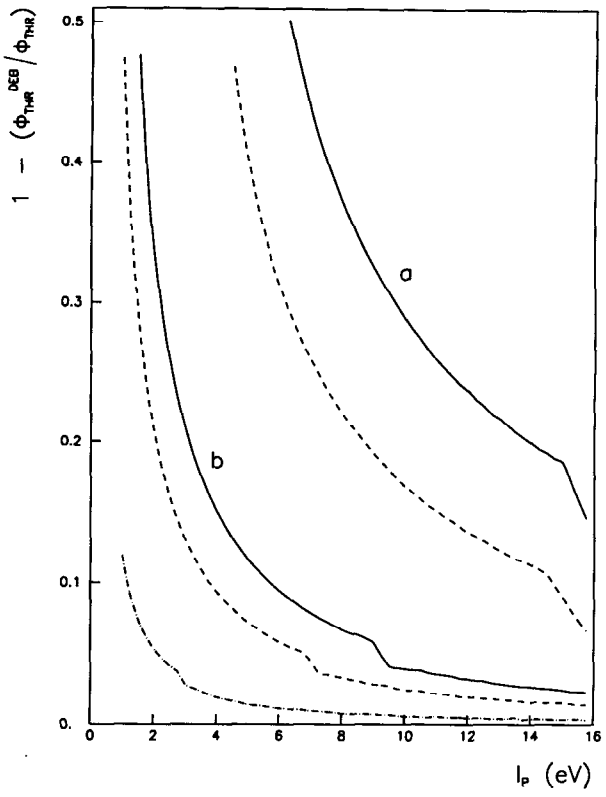

Figure 7. Relative change of the threshold energy per square centimeter is given as a function of the ionization potential using the basic adiabatic absorption model with the Debye correction.

potential energy in vacuum, the ionization energy has to be corrected for this difference.

For a distance r equal to λ_D the interaction energy of a singly charged ion and an electron is given by

$$\Delta E_D = e_0 V_{r=\lambda_D} = e_0^3 \left(\frac{8\pi n_e}{kT}\right)^{1/2} \frac{1}{e} \qquad (22)$$

and approximates the depression of the ionization energy. This value differs from that published by Drawin (*13*) by a factor of $1/e$ and gives rise to smaller corrections on the ionization energy. This reduction is reasonable since otherwise in dense plasmas the depression of ionization energy due to the screening effect exceeds the ionization potential itself.

Figure 7 shows the tendency of the relative change of the threshold as a function of the ionization potential and molar absorption coefficient. Three laser types were investigated: the quadrupled Nd-YAG laser (full line), the ruby laser (dashed line), and the CO_2 laser (dashed dotted line). Number density of the target was fixed to 5×10^{22} particles/cm^3. Absorption coefficient values were taken equal to 100 (a) and 0.1 L mol^{-1} cm^{-1} (b).

It is clear that the Debye correction is comparable in importance to the Poole–Frenkel correction. A significant difference between them is that the Debye correction is in effect even after the laser pulse has decayed while the Poole–Frenkel effect vanishes.

According to our threshold condition eq 12 a drop of the molar absorption coefficient from 100 to 0.1 L mol^{-1} cm^{-1} is related to a considerable decrease in the plasma absorption coefficient. This change is linked to a drop of the electron density through the threshold degree of ionization (50–100 times smaller). Consequently a lower threshold temperature was noticed as well (2 to 3 times smaller). Therefore, from eq 17 it can be concluded that the Debye length is raised by a factor of 5. As a result ΔE^D will be ~5 times smaller leading to a smaller relative change in the threshold in the lower absorptivity case.

Both corrections have been implemented and the results for tryptophan, nicotinic acid, and 3-nitrobenzyl alcohol are given in Table I. Threshold energies per unit area can be compared with the threshold values acquired by experiments (*5*). As we mentioned earlier, the experimental values are necessarily lower bounds for the calculated ones since their definition is related to the appearance of any kind of sample specific ion. Therefore, calculated thresholds are expected to be higher than the experimental ones. This expectation is fulfilled as one can notice from Table I.

Another feature to be mentioned is how little room is left for laser desorption between the appearance of the first desorbed ions and the takeover of plasma ionization.

Although it would be desirable, detailed comparison of our model with systematic experimental studies of ion kinetic energy distributions as a function of laser energy is not possible, since only scattered data are available.

ACKNOWLEDGMENT

A.V. is indebted to Fred Adams for his continuous inspiration and interest in the work and to David M. Hercules for providing information about his defocusing experiments and for the valuable discussions concerning their interpretation.

Registry No. Tryptophan, 73-22-3; nicotinic acid, 59-67-6; 3-nitrobenzyl alcohol, 619-25-0.

LITERATURE CITED

(1) Hillenkamp, F. In *Ion formation from organic solids*; Benninghoven, A., Ed.; Springer: Berlin, 1983; Springer Series in Chem. Phys. 25, pp 190–205.
(2) Van der Peyl, G. J. Q.; Van der Zande, W. J.; Kistemaker, P. G. *Int. J. Mass Spectrom. Ion Processes* **1984**, *62*, 51.
(3) Vertes, A.; Juhasz, P.; De Wolf, M.; Gijbels, R. *Scanning Microsc.* **1988**, *2*, 1853.
(4) Karas, M.; Bachmann, D.; Hillenkamp, F. *Anal. Chem.* **1985**, *57*, 2935.
(5) Karas, M.; Bachmann, D.; Bahr, U.; Hillenkamp, F. *Int. J. Mass Spectrom. Ion Processes* **1987**, *78*, 53.
(6) Hercules, D. M., Department of Chemistry, University of Pittsburgh, Pittsburgh, personal communication, 1988. Also *Anal. Chem.* **1988**, *60*, 2338.
(7) Vertes, A.; Juhasz, P.; Jani, P.; Czytrovszky, A. *Int. J. Mass Spectrom. Ion Processes* **1988**, *83*, 45.
(8) Mauney, T.; Adams, F. *Int. J. Mass Spectrom. Ion Processes* **1984**, *59*, 103.
(9) Michiels, E.; Mauney, T.; Adams, F.; Gijbels, R. *Int. J. Mass Spectrom. Ion Processes* **1984**, *61*, 231.
(10) Mulser, P. *Z. Naturforsch.* **1970**, *25A*, 282.
(11) Hora, H. *Nonlinear Plasma Dynamics at Laser Irradiation*; Springer: Berlin, 1979.
(12) Spitzer, L. *Physics of Fully Ionized Gases*; Interscience Publishers: London, 1956; pp 65–76.
(13) Drawin, H. W. In *Reactions under plasma conditions*; Venogupalan, M., Ed.; Wiley: New York, 1971; Vol. I, pp 53–238.
(14) Coelho, R. *Physics of Dielectrics for the Engineer*; Elsevier: Amsterdam, 1979; pp 136–142.
(15) *Handbook of Optical Constants of Solids*; Palik, E. D., Ed.; Academic: Orlando, FL, 1985; pp 275–804.
(16) *CRC Handbook of Chemistry and Physics*; Weast, R. C., Ed.; CRC Press: Boca Raton, FL, 1983.
(17) Vedeneyev, V. I.; Gurvich, L. V.; Kondrat'yev, V. N.; Medvedev, V. A.; Frankevich, Ye. L. *Bond Energies, Ionization Potentials and Electron Affinities*; Edward Arnold (Publishers) Ltd.: London, 1966; pp 151–190.
(18) Levin, R. D.; Lias, S. G. *Ionization Potential and Appearance Potential Measurements, 1971–1981*; NSRDS-NBS 71; U.S. Government Printing Office: Washington, DC, 1982; pp 1–634.

RECEIVED for review June 28, 1988. Accepted January 23, 1989. This work was partly supported by the Belgian Nationaal Fonds voor Wetenschappelijk Onderzoek.